Network Representation of Higher-Order Interactions Based on Information Dynamics

Gorana Mijatovic, *Member, IEEE*, Yuri Antonacci, *Member, IEEE*, Michal Javorka, Daniele Marinazzo, Sebastiano Stramaglia, and Luca Faes, *Senior Member, IEEE*

Abstract—Many complex systems in science and engineering are modeled as networks whose nodes and links depict the temporal evolution of each system unit and the dynamic interaction between pairs of units, which are assessed respectively using measures of auto- and cross-correlation or variants thereof. However, a growing body of work is documenting that this standard network representation can neglect potentially crucial information shared by three or more dynamic processes in the form of higher-order interactions (HOIs). While several measures, mostly derived from information theory, are available to assess HOIs in network systems mapped by multivariate time series, none of them is able to provide a compact yet detailed representation of higher-order interdependencies. In this work, we fill this gap by introducing a framework for the assessment of HOIs in dynamic network systems at different levels of resolution. The framework is grounded on the dynamic implementation of the O-information, a new measure assessing HOIs in dynamic networks, which is here used together with its local counterpart and its gradient to quantify HOIs respectively for the network as a whole, for each link, and for each node. The integration of these measures into the conventional network representation results in a tool for the representation of HOIs *as networks*, which is defined formally using measures of information dynamics, implemented in its linear version by using vector regression models and statistical validation techniques, illustrated in simulated network systems, and finally applied to an illustrative example in the field of network physiology.

Index Terms—higher-order networks, synergy and redundancy, information theory, time series analysis, network physiology

1 Introduction

Complex systems consisting of many interacting units are commonly depicted as networks, according to a paradigm widely used to investigate the structure and dynamics of several real-world phenomena [1]. The classical network representation of dynamic systems makes use of nodes, associated to system units and possibly representing temporal dependencies of the unit activity, and links, representing functional dependencies between pairs of units. This representation encoding so-called lower-order interactions (LOIs) is ubiquitous in many fields of science and engineering, as it applies to social systems [2], electronic oscillators [3], ecosystems and climate systems [4], as well as neuroscience and physiology [5], [6]. However, it has now firmly established that in all these systems interactions can occur in groups of three or more nodes, giving rise to collective dynamics known as higher-order interactions (HOIs) that cannot be fully accounted by single-node and pairwise dynamic measures [7].

HOIs manifest themselves in complex network systems both at the level of *mechanisms*, through the presence of higher-order terms in generative models of the dynamics at each node, and at the level of *behaviors*, through the emergence of higher-order correlations in the multivariate dynamic processes mapping the system evolution [8]. Since the dynamics of networks with HOI mechanisms differ substantially to those generated solely by LOI mechanisms [9], [10], it is evident that higher-order mechanisms shape in a significant way the behavior of network systems. Nevertheless, higher-order behaviors can emerge even in systems without higher-order mechanisms [8]. It is therefore imperative, to fully characterize the dynamic behavior of complex network systems, to move from the use of standard LOI measures to the adoption of frameworks able to depict the various types of HOIs that emerge within the resulting multivariate statistics.

The detection of HOIs from the behavior of network systems embodies the statistical concepts of synergy and redundancy, and is typically formalized into the frame of partial information decomposition and its various developments [11], [12]. Information-theoretic tools play a main role in this context, with the mutual information (MI) being the primary measure to capture pairwise interactions and its multivariate extensions serving as measures of higher-order behaviors. Among the latter, the long-known measure of interaction information (II) [13] quantifies HOIs in terms of the synergy/redundancy balance among three random variables. The II has been recently extended to an arbitrary number of variables through the concept of O-information (OI) [14], [15]. The MI, II, and OI are effective for describing static networks represented by random variables, but they

- *G. Mijatovic is with the Faculty of Technical Sciences, University of Novi Sad, Serbia. E-mail: gorana86@uns.ac.rs*
- *Y. Antonacci is with the Department of Engineering, University of Palermo, Italy*
- *M. Javorka is with the Department of Physiology and Biomedical Center Martin, Jessenius Faculty of Medicine, Comenius University, Slovakia*
- *D. Marinazzo is with the Department of Data Analysis, University of Ghent, Belgium*
- *S. Stramaglia is with the Department of Physics, University of Bari Aldo Moro, and INFN Sezione di Bari, Italy*
- *L. Faes is with the Department of Engineering, University of Palermo, Italy, and the Faculty of Technical Sciences, University of Novi Sad, Serbia. E-mail: luca.faes@unipa.it*

fall short in capturing the dynamics of networks that evolve over time, which typically exhibit autocorrelations and time-lagged cross-correlations. This limitation can be addressed through the introduction of approaches measuring dynamic information rates, rather than static information quantities, for the analysis of higher-order behaviors [16], [17]; the resulting measures, i.e. the MI rate (MIR), II rate (IIR), and OI rate (OIR), extend the analysis of HOIs to dynamic networks characterized by random processes.

In this context, the aim of the present study is to introduce a framework for the comprehensive description of different types of high-order behaviors in network systems mapped by multivariate time series. The framework is grounded on the OIR and related measures, which are formulated in this work to assess HOIs operating simultaneously across different levels of resolution: the entire network, individual links, and specific nodes. We use the OIR as a global, network-wise measure capturing HOIs among all the analyzed processes. Further, as the OIR cannot consider higher-order effects that are specific to certain parts of the network (e.g., individual nodes or links), we introduce into the framework two additional HOI descriptors: the local OIR, quantifying the net information shared between two processes and the rest of the network [18], here taken as link-wise measure of HOIs; and the OIR-gradient [19], quantifying the information shared between one process and the rest of the network. This new framework allows to capture different types of high-order behaviors simultaneously and in a compact way (i.e., through the use of a single HOI measure for each node/link), so as to represent them *as networks* investigated across different levels of resolution.

The rest of this paper is organized as follows. First, we provide the theoretical formulation of OIR, local OIR and OIR-gradient (Sect. 2.1), and derive a data-efficient implementation of all measures based on linear vector autoregressive (VAR) models (Sect. 2.2), as well as methods to estimate them from multivariate time series (Sect. 2.3) and to assess their statistical significance (Sect. 2.4). Then, the framework is illustrated in benchmark simulated network systems, showing how the proposed dynamic HOI measures can evidence collective behaviors not revealed by LOI descriptors and depict them more reliably than baseline HOI measures (Sect. 3). Finally, the framework is employed to investigate both LOIs and HOIs in an application very common in computational and network physiology [5], [20], [21], i.e. the study of heart rate, arterial pressure and vascular resistance time series measured on a beat-by-beat basis from multiple biosignals (Sect. 4); the resulting cardiovascular networks are here investigated in healthy subjects monitored in a resting state and during postural and mental stress, to showcase the relevance of HOIs in the homeostatic regulation analyzed across different physiological states.

2 METHODS

2.1 Framework to Assess Higher-Order Interactions at Different Levels of Resolution

Let us consider a dynamic network system $\mathcal{X}$ composed of N nodes, whose activity is described by N discrete-time random processes $X = \{X_1, \dots, X_N\}$. The average rate of information produced over time by the process X_i, which maps the activity of the i^{th} node of the network, is quantified by its entropy rate (ER). The ER captures the internal dynamics of the process, i.e., its self-interactions of order one. For a stationary process X_i, the ER is [22]:

$$H_{X_i} = \lim_{k\to\infty} \frac{1}{k} H(X_{i,n-k:n-1}) = H(X_{i,n}|X^-_{i,n}), \quad (1)$$

where $X_{i,n}$, $X_{i,n-k:n-1}$, and $X^-_{i,n} = \lim_{k\to\infty} X_{i,n-k:n-1}$ denote the random variables sampling X_i at the present time n, over the past k lags, and over the whole past history, respectively. The second equality in Eq. (1) expresses the ER as a conditional entropy, evidencing the amount of information contained in the present time of the process X_i that cannot be explained by its past. As such, the ER serves as a measure for assessing the complexity of the process dynamics: if X_i is a fully random process, it produces information at the maximum rate, resulting in the maximum ER; if, on the contrary, X_i is a fully predictable process, it does not produce new information and its ER is null.

The interactions of order two between the i^{th} and j^{th} nodes of the analyzed network can be assessed by the mutual information rate (MIR) of the processes X_i and X_j. The MIR quantifies dynamic coupling measuring the information shared by the processes per unit of time [23]:

$$I_{X_i;X_j} = \lim_{k\to\infty} \frac{1}{k} I(X_{i,n-k:n-1}; X_{j,n-k:n-1}), \quad (2)$$

$$= H_{X_i} + H_{X_j} - H_{X_i,X_j}, \quad (3)$$

where H_{X_i} and H_{X_j} are the ERs of the processes X_i and X_j, and H_{X_i,X_j} is the joint ER of the two processes.

The ER and MIR measures quantify the intensity of lower-order interactions (LOIs) in the network system, i.e. interactions within and between processes that are encoded respectively by nodes and links in the standard network representation (Fig. 1a). In this work, ER and MIR serve also as building blocks for computing measures of higher-order interactions (HOIs) in the analyzed dynamic network. Here, using ER and MIR we introduce a comprehensive framework for the evaluation of different types of interactions beyond pairwise connections. The framework is grounded on the so-called O-information rate (OIR), a measure capturing the net information shared in network of random processes [16]. Specifically, the OIR (Ω) of the N processes grouped in X can be defined combining the entropy rates of the processes as:

$$\Omega_X = (N-2)H_X + \sum_{j=1}^{N} [H_{X_j} - H_{X^j}], \quad (4)$$

where $X^j = X \backslash \{X_j\}$ is the vector process including the activity of all network nodes except X_j. The OIR quantifies the collective interactions between all processes analyzed. It can be also computed iteratively from the OIR of the subset X^j including $N-1$ processes by summing a gradient (Δ) which quantifies the informational increment obtained when X_j is added to X^j [16]:

$$\Omega_X = \Omega_{X^j} + \Delta_{X_j;X^j}, \quad (5)$$

$$\Delta_{X_j;X^j} = \sum_{\substack{i=1 \\ i\neq j}}^{N} I_{X_j;X^{ij}} + (2-N) I_{X_j;X^j}. \quad (6)$$

Note that the OIR is zero if $N = 2$, while for $N = 3$ it is equal to the OIR-gradient, which in turn corresponds to the so-called interaction information rate (IIR), i.e. $\Omega_X = \Delta_{X_j;X^j} = I_{X_i;X_j;X_k} = I_{X_i;X_j} + I_{X_k;X_j} - I_{X_i,X_k;X_j}$ $(i \neq j \neq k \in \{1,2,3\})$ [16]. Further, when networks mapped by more than three random processes are analyzed, the IIR can be generalized by focusing on two processes X_i and X_j and collecting all other processes in the vector $X^{ij} = X \backslash \{X_i, X_j\}$; the resulting measure is the dynamic version of the local OI defined in [14], also denoted as net information shared in [18]:

$$I_{X_i;X_j;X^{ij}} = I_{X_i;X_j} + I_{X_i;X^{ij}} - I_{X_i;X^i}. \tag{7}$$

Importantly, all the measures defined in Eqs. (4), (6), (7) quantify HOIs by capturing the balance between *redundancy* and *synergy*: they take positive values when redundant interactions prevail over synergistic interactions, and negative values in the opposite case. Here, the terms "redundant" and "synergistic" applied to multivariate information measures refer respectively to information identically provided by each of the multiple analyzed units, and to new information that emerges when the units are considered together. Building on these measures, our framework explores HOIs within the observed network system across multiple levels of spatial resolution. This spatially-resolved representation of HOIs includes different descriptors (Fig. 1b):

- *Node-wise*, based on the OIR-gradient (Eq. 6) quantifying the informational character (redundant or synergistic) provided by the inclusion of the analyzed node into the multiplet formed by all other network nodes;
- *Link-wise*, HOIs based on the local OIR (Eq. 7) quantifying the net information shared between the two analyzed nodes and the rest of the network;
- *Network-wise*, based on the OIR (Eq. 4) quantifying the redundant/synergistic character of the overall dynamic interactions among all the network nodes.

Collectively, these descriptors provide a representation of HOIs as networks which guarantees lower computational complexity compared to existing representations (e.g., [24]). In fact, for a network of N nodes, our framework computes N OIR-gradient values, $\frac{N(N-1)}{2}$ local-OIR values, and one OIR value; this is a considerably smaller number of HOI measures to be computed compared with standard approaches for which such number grows exponentially with the network size (e.g., the number of multiples of order M in a network with N nodes scales factorially with the binomial coefficient $C_{N,M} = \frac{N!}{M!(N-M)!}$).

2.2 Computation for Linear Systems

This section presents the implementation of the proposed framework using linear vector autoregressive (VAR) models [25]. Crucially, the use of VAR models induces a linear representation of the analyzed process without forcing the assumption that it must be linear, as any stationary process can be decomposed into a linear model [26]. The VAR representation of the zero-mean process X is given by:

$$X_n = \sum_{k=1}^{p} \mathbf{A}_k X_{n-k} + U_n, \tag{8}$$

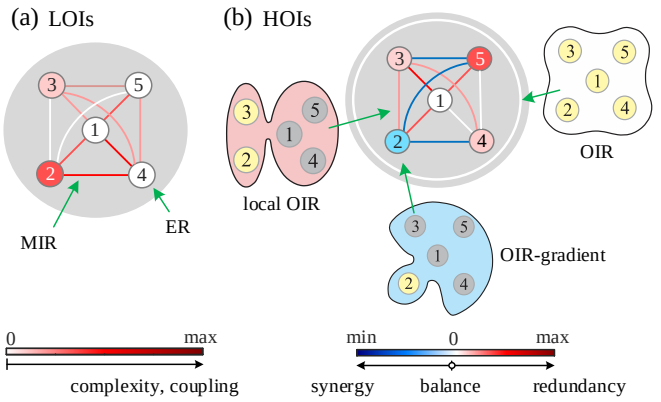

Fig. 1. Exemplary illustration of a network system with five nodes showing the network representation of lower-order interactions (LOIs) and higher-order interactions (HOIs). (a) LOI measures quantify the information produced at each node (entropy rate (ER), related to process complexity) and the information shared per unit of time between any two nodes (mutual information rate (MIR), related to coupling between processes), which are coded respectively by the color of the nodes and of the links. (b) HOI measures quantify the net information shared per unit of time among all network nodes, reflecting higher-order behaviors related to the synergy/redundancy balance evaluated at the level of the whole network (O-information rate, OIR), single link (local OIR), and single node (OIR-gradient), which are coded respectively by the color of the external circle, of the links, and of the nodes. In the example, the process X_2 is involved in LOIs (a) showing the highest complexity (red color of node 2), strong coupling with X_4 (red link 2-4) and uncoupling with X_3 (white link 2-3), while it is involved in HOIs (b) providing synergy if considered alone (blue node 2 and OIR-gradient hyperlink), providing redundancy if considered with X_3 (red link 2-3 and local-OIR hyperlink), and participating to the collective synergy/redundancy balance (white external circle and OIR hyperlink).

where p is the model order, X_n and X_{n-k} are the $N-$dimensional variables sampling the process X at the present time n and at k lags in the past, $\mathbf{A}_k$ are $N \times N$ coefficient matrices encoding the causal relations from past to present for each lag k, and U is an i.i.d. innovation process with $N \times N$ covariance matrix $\mathbf{\Sigma}_U = \mathbb{E}[U_n U_n^\intercal]$.

Starting from the ubiquitous representation in Eq. (8), developments of the theory of Granger causality have shown that it is possible to define *restricted* models which describe the dynamics of properly chosen subsets of processes [27]. Specifically, the dynamics of the generic sub-process $Y \subset X$ collecting M scalar processes taken from X (typically, $M < N$) are described by the restricted model:

$$Y_n = \sum_{k=1}^{q} \mathbf{B}_k Y_{n-k} + W_{Y,n}, \tag{9}$$

where W_Y is the M-dimensional innovation process feeding the restricted model to yield the analyzed sub-process Y, and $\mathbf{B}_k$ are the relevant $M \times M$ coefficient matrices; note that the order of the restricted model q will generally tend to infinity because a sub-process of a VAR process will have a moving average component [28]. Importantly, under the assumption of joint Gaussianity for the overall process X, the ER of the sub-process Y can be derived straightly based on the generalized variance of the residuals of the restricted model of Eq. (9) as follows [17]:

$$H_Y = \frac{1}{2} \log(2\pi e)^M |\mathbf{\Sigma}_{W_Y}|, \tag{10}$$

where $\mathbf{\Sigma}_{W_Y} = \mathbb{E}[W_{Y,n}W_{Y,n}^\intercal]$ is the $M \times M$ covariance matrix of the restricted innovation process W_Y. Moreover, considering another sub-process $Z \subset X$ disjoint from Y, and considering the joint process $[YZ] = Y \cup Z$, similar formulations like in Eqs. (9) and (10) can be written and combined to derive the MIR between Y and Z as follows:

$$I_{Y;Z} = \frac{1}{2}\log\frac{|\mathbf{\Sigma}_{W_Y}||\mathbf{\Sigma}_{W_Z}|}{|\mathbf{\Sigma}_{W_{YZ}}|}. \tag{11}$$

Eqs. (10) and (11) are the cornerstone for the computation of information dynamic measures based on VAR models. In fact, the ER of the scalar process X_i is obtained simply by assuming $Y = X_i$ in Eq. (10):

$$H_{X_i} = \frac{1}{2}\log 2\pi e\Sigma_{W_{X_i}}; \tag{12}$$

the MIR between the processes X_i and X_j is obtained simply by assuming $Y = X_i$ and $Z = X_j$ in Eq. (11):

$$I_{X_i;X_j} = \frac{1}{2}\log\frac{\Sigma_{W_{X_i}}\Sigma_{W_{X_j}}}{|\mathbf{\Sigma}_{W_{X_iX_j}}|}; \tag{13}$$

and the local OIR between X_i and X_j given X^{ij} is derived applying Eq. (13) three times according to Eq. (7) to yield:

$$I_{X_i;X_j;X^{ij}} = \frac{1}{2}\log\frac{\Sigma_{W_{X_i}}\Sigma_{W_{X_j}}|\mathbf{\Sigma}_{W_{X^{ij}}}||\mathbf{\Sigma}_U|}{|\mathbf{\Sigma}_{W_{X_{ij}}}||\mathbf{\Sigma}_{W_{X^j}}||\mathbf{\Sigma}_{W_{X^i}}|}. \tag{14}$$

With similar reasoning, the OIR among all processes in X can be derived from Eq. (4) using the formulation of the ER (Eq. 10), one time with $Y = X$ and repeatedly with $Y = X_j$ and $Y = X^j$, and the OIR-gradient of the process X_j given the other processes X^j can be derived from Eq. (6) using the formulation of the MIR (Eq. (11), one time with $\{Y = X_j, Z = X^j\}$ and repeatedly with $\{Y = X_j, Z = X^{ij}\}$.

2.3 Estimation

The parameters of the restricted model (Eq. 9), i.e. the coefficients $\mathbf{B}_k$ and the covariance of the residuals $\mathbf{\Sigma}_{W_Y}$, can be derived from the parameters of the full model (Eq. 8), $\mathbf{A}_k$ and $\mathbf{\Sigma}_U$, through a two-step procedure which (i) derives the time-lagged covariance structure of the full process X, and (ii) reorganizes such structure to relate it to the covariance of the sub-process Y [29].

The step (i) exploits the fact that the covariance of X, $\mathbf{\Sigma}_{X,k} = \mathbb{E}[X_nX_{n-k}^\intercal]$, is related to the VAR parameters via the well-known Yule-Walker equations [25]:

$$\mathbf{\Sigma}_{X,k} = \sum_{l=1}^{p}\mathbf{A}_l\mathbf{\Sigma}_{X,k-l} + \delta_{k0}\mathbf{\Sigma}_U, \tag{15}$$

where δ_{k0} is the Kronecher delta function. To solve this equation for $k = 0, 1, \ldots, p-1$, we first express Eq. (8) in a compact form as $X_n^p = \mathbf{A}^pX_{n-1}^p + U_n^p$, where

$$X_n^p = \left[X_n^\intercal X_{n-1}^\intercal \cdots X_{n-p+1}^\intercal\right]^\intercal, \tag{16a}$$

$$\mathbf{A}^p = \begin{bmatrix}\mathbf{A}_1 & \cdots & \mathbf{A}_{p-1} & \mathbf{A}_p\\ \mathbf{I} & \cdots & \mathbf{0} & \mathbf{0}\\ \vdots & \ddots & \vdots & \vdots\\ \mathbf{0} & \cdots & \mathbf{I} & \mathbf{0}\end{bmatrix}, \tag{16b}$$

$$U_n^p = \left[U_n^\intercal \mathbf{0}\right]^\intercal. \tag{16c}$$

Then, the covariance matrix of X_n^p, $\mathbf{\Sigma}_X^p = \mathbb{E}[X_n^pX_n^{p\intercal}]$, which has the form:

$$\mathbf{\Sigma}_X^p = \begin{bmatrix}\mathbf{\Sigma}_X & \mathbf{\Sigma}_{X,1} & \cdots & \mathbf{\Sigma}_{X,p-1}\\ \mathbf{\Sigma}_{X,1}^\intercal & \mathbf{\Sigma}_X & \cdots & \mathbf{\Sigma}_{X,p-2}\\ \vdots & \vdots & \ddots & \vdots\\ \mathbf{\Sigma}_{X,p-1}^\intercal & \mathbf{\Sigma}_{X,p-2}^\intercal & \cdots & \mathbf{\Sigma}_X\end{bmatrix}, \tag{17}$$

can be expressed as:

$$\mathbf{\Sigma}_X^p = \mathbf{A}^p\mathbf{\Sigma}_X^p(\mathbf{A}^p)^\intercal + \mathbf{\Sigma}_U^p, \tag{18}$$

which is a discrete-time Lyapunov equation ($\mathbf{\Sigma}_U^p$ denotes the covariance of U_n^p, i.e., $\mathbf{\Sigma}_U^p = \mathbb{E}[U_n^pU_n^{p\intercal}]$). The Lyapunov equation can be solved for $\mathbf{\Sigma}_X^p$, thus yielding the covariance matrices $\mathbf{\Sigma}_X, \mathbf{\Sigma}_{X,1}, \cdots, \mathbf{\Sigma}_{X,p-1}$. Then, the covariance can be calculated recursively for any lag $k \geq p$ by applying Eq. (15), so as to obtain $\mathbf{\Sigma}_{X,p}, \mathbf{\Sigma}_{X,p+1}, \cdots, \mathbf{\Sigma}_{X,q}$.

The step (ii) of the estimation procedure starts with extracting, from the covariance matrices $\mathbf{\Sigma}_{X,k}$ computed for each lag $k \in \{0, 1, \ldots, q\}$, only the covariance elements relevant to the sub-process Y, which form the covariance matrices $\mathbf{\Sigma}_{Y,k} = \mathbb{E}[Y_nY_{n-k}^\intercal]$. These covariances are arranged to obtain the covariance matrix of Y, $\mathbf{\Sigma}_Y = \mathbb{E}[Y_nY_n^\intercal]$, the covariance of the predictors of Eq. (9), $\mathbf{\Sigma}_Y^q = \mathbb{E}[Y_n^qY_n^{q\intercal}]$, and the cross-covariance $\mathbf{\Sigma}_{Y_n;Y_{n-1}^q} = \mathbb{E}[Y_nY_{n-1}^{q\intercal}]$ (where $Y_{n-1}^q = \left[Y_{n-1}^\intercal \cdots Y_{n-q}^\intercal\right]^\intercal$). Finally, solving the Yule-Walker equations, the coefficients of the restricted model are computed as $\mathbf{B}_k = \mathbf{\Sigma}_{Y_n;Y_n^q}{\mathbf{\Sigma}_Y^q}^{-1}$, and the covariance matrix of the residuals is obtained as [29]:

$$\mathbf{\Sigma}_{W_Y} = \mathbf{\Sigma}_Y - \mathbf{\Sigma}_{Y_n;Y_n^q}{\mathbf{\Sigma}_Y^q}^{-\intercal}\mathbf{\Sigma}_{Y_n;Y_n^q}^\intercal. \tag{19}$$

The procedure described above starts from the VAR parameters $\mathbf{A}_k$ and $\mathbf{\Sigma}_U$ of the full model, which can be easily estimated from realizations of the process X available in the form of multivariate time series. While advanced procedures exist to perform VAR model identification, e.g. using penalized regression to derive sparse models in high-dimensional settings [30] or using time-varying regression to derive time-dependent parameters in non-stationary conditions [31], the classical least squares approach was followed in this work [25]. The order p of the full model is typically estimated using information-theoretic criteria, like the Akaike [32], or the Bayesian [33], while the order q of the restricted models is set at high values to capture the decay of the correlations at increasing lags [27], [29].

2.4 Statistical Significance

This section describes the approach followed to statistically validate measures of the OIR-gradient, local OIR, and OIR, i.e., to determine if an estimated value of any of these measures can be regarded as significantly different from zero, detecting the presence of net redundancy if positive and of net synergy if negative. In this work, a procedure based on the bootstrap technique [34] was implemented, exploiting the fact that the HOI measures can take both positive and negative values. Specifically, for any given multivariate time series, a VAR model was identified by the least squares method, and bootstrap pseudo-series were created by feeding the identified model with new realizations of the innovations U obtained by repeatedly sampling with

replacement from the estimated innovations. This procedure ensures that the bootstrap series retain all characteristics of the original process X, including causal relationships and zero-lag correlations. Then, the OIR-gradient, local OIR and OIR are computed from the bootstrap realizations. The procedure is repeated several times to construct bootstrap distributions of each HOI measure, whose confidence intervals are finally used to assess the statistical significance of each original estimate of the measure. Setting a significance level α, if the zero level falls between the $(100 \cdot \alpha/2)^{th}$ and $(100 \cdot (1-\alpha/2))^{th}$ percentiles of the bootstrap distribution of the HOI measure, the measure itself is considered as non-significant; otherwise, it is deemed as significant [35].

As regards the statistical significance of the MIR estimates, the bootstrap technique cannot be followed because any MIR estimate takes only positive values. In this case, the method of surrogate data was employed, generating iterative amplitude-adjusted Fourier Transform surrogates [36] of each set of original time series. While preserving the individual properties (amplitude distribution, autocorrelation structure) of each original time series, these surrogates are fully uncoupled, thus adhering to the null hypothesis of uncorrelated time series for which the MIR is absent. The rejection of this null hypothesis occurs with significance α when the MIR estimated on the original series exceeds the $(100 \cdot (1-\alpha))^{th}$ percentile of the surrogate distribution.

3 Validation on Simulations

In this section, we illustrate the framework described above in simulated dynamic networks whose activity is mapped by a multivariate random process described by a VAR model. Specifically, we first consider two simulation settings in which the network measures are computed analytically from the theoretical values imposed for the model parameters; these simulations are designed to highlight the importance of assessing dynamic HOIs in multivariate processes with temporal correlations (Sect. 3.1, comparison between static and dynamic HOI measures), and the role of HOIs beyond the standard LOI description (Sect. 3.2, comparison between HOI and LOI measures). Then, in Sect. 3.3 the dynamic HOI measures are estimated from simulated finite-length realizations of the simulated network process, and their statistical significance is assessed as a function of the time series length.

In our simulations, we consider $N = 5$ processes interacting in a star structure, where node 1 and nodes 2-5 act respectively as the hub and as leaves. The processes are described by a VAR model fed by independent Gaussian innovations with zero mean and unit variance, formulated as in Eq. (8) with order $p = 1$. In the different simulation settings, the VAR model is identified imposing values for the time-lagged coefficients collected in the matrix $\mathbf{A}_1$ and for the elements of the innovation covariance $\mathbf{\Sigma}_U$. In the graphical network representations of Figs. 2-4, these parameter values are depicted with dashed lines when they refer to zero-lag instantaneous effects (off-diagonal elements of $\mathbf{\Sigma}_U$), with green or orange arrows when they refer to time-lagged causal effects originating from the hub or directed to it (off-diagonal elements of $\mathbf{A}_1$), and with blue arrows when they refer to self-dependencies within a process (diagonal elements of $\mathbf{A}_1$).

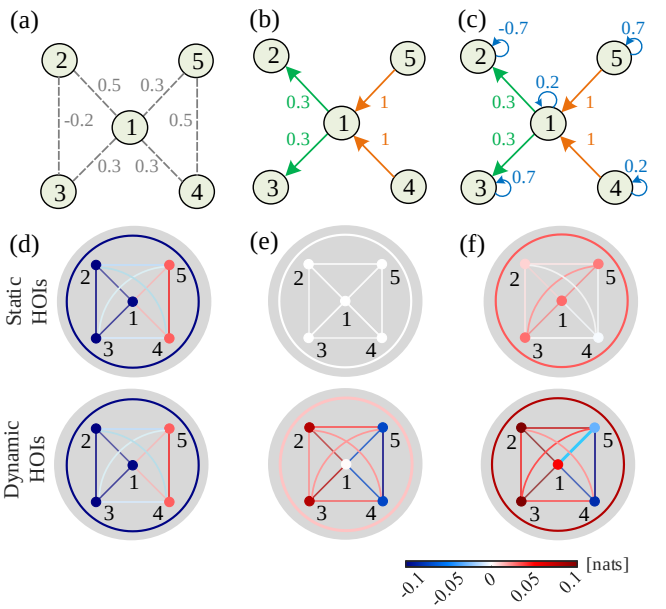

Fig. 2. Simulated networks of random processes connected via a hub (node 1) communicating with four leaves (nodes 2-5), featuring exclusive instantaneous interactions (a) and exclusive time-lagged interactions with only causal effects (b) or with both causal effects and self-dependencies (c). The higher-order networks mapping the theoretical values of OI gradient, local OI and OI measuring static HOIs, as well as the values of OIR gradient, local OIR and OIR measuring dynamic HOIs, are shown in (d-f) for the three configurations; the values of OI/OIR gradient, local OI/OIR and OI/OIR are encoded respectively by the nodes, links and external circle, with a pseudo-color representation whereby shades of blue denote synergy, shades of red denote redundancy and white denotes synergy/redundancy balance or absence.

3.1 Comparison of Static and Dynamic HOIs Measures

First, to compare static and dynamic HOIs measures, we analyze the three following configurations: (i) exclusive instantaneous interactions between the hub and all leaves, and between nodes 2-3 and 4-5 (Fig. 2a); (ii) exclusive time-lagged causal interactions, with causal effects originating from nodes 4,5, mediated by the hub and directed to nodes 2,3 (Fig. 2b); (iii) exclusive time-lagged interactions with both causal and self-effects, with causal effects between processes set as in (ii) and self-effects occurring in all processes (Fig. 2c). The first configuration is obtained imposing absence of time-lagged effects ($\mathbf{A}_1 = \mathbf{0}$), so as to simplify the VAR model to a zero-lag process with covariance $\mathbf{\Sigma}_X = \mathbf{\Sigma}_U$ (non-zero elements of $\mathbf{\Sigma}_X$ in Fig. 2a). The configurations (ii) and (iii) realize VAR models without instantaneous effects ($\mathbf{\Sigma}_U = \mathbf{I}$; non-zero elements of $\mathbf{A}_1$ in Fig. 2b,c).

For all three configurations, we built HOI networks comparing the proposed dynamic framework defined for random processes with the static analysis of HOIs defined for random variables. The dynamic analysis was performed applying to the vector process X the OIR-gradient, local OIR and OIR computed from the theoretical values of the VAR parameters according to the procedures described in Sect. 2.1-2.3. The static analysis was performed applying baseline information measures like MI, II and OI [13], [37] on the vector variable X_n sampling all the processes in X

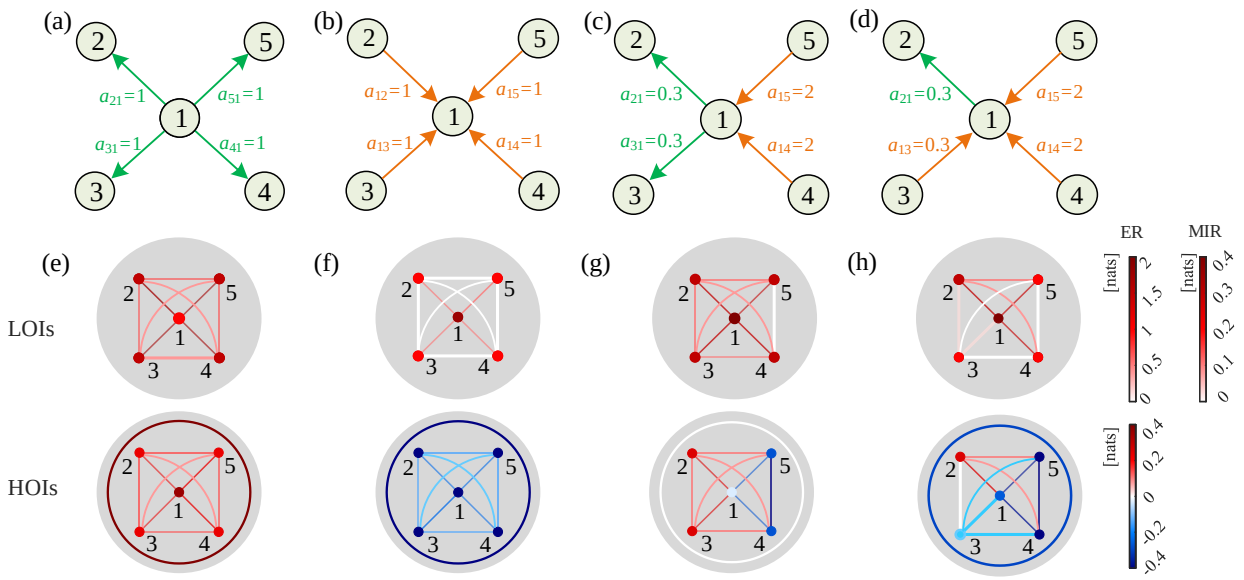

Fig. 3. Simulated network of random processes connected via a hub (node 1) communicating with four leaves (nodes 2-5), where the hub acts: as a source of information to all leaves (a); as a sink of information from all leaves (b); as a mediator of the information received from nodes 4,5 and sent to nodes 2,3 (c), or received from nodes 3,4,5 and sent to node 2 (d). The lower-order networks mapping the theoretical values of ER and MIR, measuring complexity and coupling and encoded by nodes and links, as well as the higher-order networks mapping the values of OIR gradient, local OIR and OIR, measuring the synergy/redundancy balance at different levels of spatial resolution and encoded by nodes, links and external circle, are shown in (e)-(h) for the four configurations. Each LOIs or HOIs measure is represented using pseudo-colors: in the case of LOIs, the scale ranges from white (zero) to different shades of red reflecting the measure's strength, while for HOIs it encompasses different shades of blue, white and red denoting respectively net synergy, balance and net redundancy.

at the same time n to compute measures of OI-gradient, local OI and OI; details of the implementation of these static measures starting from the VAR parameters are provided in the Appendix. The comparison indicates that, when only instantaneous interactions are simulated (Fig. 2a), the dynamic HOI description reduces to the static one (Fig. 2d), yielding exactly the same values for OI and OIR, local OI and local OIR, and OI-gradient and OIR gradient. Such measures highlight a heterogeneous distribution of HOIs, with nodes 1-2-3 and their links revealing synergy and nodes 4-5 and their links with node 1 revealing redundancy, as is expected for this type of static interactions [38]; the overall HOIs investigated at the network level document the dominance of sinergy (blue external circle).

When the simulated interactions are time-lagged (Fig. 2b,c), the static HOI description becomes unreliable and only the dynamic description fully captures the nature of high-order effects in the network. Indeed, depending on the nature and extent of the temporal correlations within the network, the HOI analysis based on the static descriptors may either fail to capture any higher-order behavior (Fig. 2e, where the OI, local OI and OI gradient measures are all identically null) or provide misleading information about higher-order behaviors (Fig. 2f, where the OI gradient and local OI suggest slightly redundant or balanced HOI). On the contrary, the dynamic analysis indicates that in both cases HOIs follow an heterogeneous spatial distribution, with an overall prevalence of redundancy (positive values of global OIR, and of OIR gradient and local OIR involving nodes 2 and 3), but also an evident synergistic circuit (negative values of OIR gradient and local OIR related to how nodes 4 and 5 interact with the hub). The heterogeneous distribution of HOIs documented only by the dynamic measures in Fig. 2e,f is compatible with the structure of the interactions simulated in 2b,c. Such structure realizes a so-called "common driver" effect with the influence of node 1 on nodes 2,3, and a "common target" effect with the influence of nodes 4,5 on node 1; these effects are known to generate higher-order behaviors with dominance of redundancy in the case of common driver, and dominance of synergy in the case of common target [18].

3.2 Comparison of HOI and LOI Measures

Next, we investigate how dynamic HOIs arise from different network topologies and compare them with the standard LOI representation. To this end, we analyze the simulated VAR processes connected through a star structure, considering four different configurations in which the hub (node 1) acts: as a *source*, sending information to all leaves (Fig. 3a); as a *sink*, receiving information from all leaves (Fig. 3b); and as a *mediator*, sending to nodes 2-3 the information received from nodes 4-5 (Fig. 3c), or sending to node 2 the information received from nodes 3-5 (Fig. 3d). The analysis of dynamic LOIs and HOIs was performed computing the ER and MIR at the node- and link-wise levels, as well as the OIR-gradient, local OIR and OIR at the node-, link- and network-wise levels, from the theoretical values of the VAR parameters imposed for each network configuration.

The resulting LOI and HOI networks obtained for the four configurations are shown in Fig. 3e-h. The analysis of lower-order behaviors (Fig. 3e-h, upper panels) evidences the presence of complex dynamics underlying the activity at each network node, documented by the relatively high values of the ER of the node dynamics, and of a fully connected network with the hub coupled to each leaf, documented by the significant values of the MIR between

node 1 and nodes 2-5. As expected by the use of pairwise interaction measures [18], the MIR detects the existing links between the hub and each leaf but also several spurious links between leaves originating from topological common driver or cascade effects (e.g., Fig. 3e,g,h). The overall similar connectivity patterns found consistently across the four configurations suggest the limited capability of LOI analysis to detect emergent dynamic behaviors distinctive of the different network topologies.

On the other hand, the analysis of higher-order behaviors (Fig. 3e-h, lower panels) documents the capability of the proposed framework to capture the informational character of multivariate interactions among hub and leaves at different levels of spatial resolution, distinguishing the different network topologies underlying the various configurations analyzed. Specifically, when the hub is a source of information for all leaves, all HOI measures reveal the predominance of redundant interactions, induced by the simulation of multiple common driver effects (Fig. 3e). When the hub is a sink of information arriving from the leaves, all measures reveal the synergistic character of HOIs at all levels of resolution, arising from the presence of multiple common target effects (Fig. 3f). In the two other configurations with the hub acting as a mediator, the presence of common driver, cascade and common target effects determines an heterogeneous distribution of HOIs, with nodes 4-5 and their connected links indicating synergy, and node 2 and its connected links indicating redundancy (Fig. 3g,h).

The comparison between lower- and higher-order networks suggests that the balance between redundancy and synergy captured by HOIs is related to the density of the LOI networks: in highly connected LOI networks where common driver and/or cascade effects induce spurious links, HOI networks are mostly redundant (Fig. 3e,g); in more sparse LOI networks where common target effects highlight the true links only, HOI networks display synergy (Fig. 3f,h). This spatially-resolved information about HOIs is provided by the OIR gradient and the local OIR at the level of nodes and links, while the global OIR captures the overall net information shared which can be redundant (Fig. 3e), balanced (Fig. 3g) or synergistic (Fig. 3f,h).

3.3 Analysis on simulated time series

Here we report the practical analysis of the investigated network process, realized in the configuration where the hub acts as a mediator of information flow (Fig. 4a). The time-lagged coefficients were set as indicated in Fig. 4a, with the coefficient a_{31} varying between 0 and 0.3 to simulate the transition from a network with an isolated node to the network already analyzed in Fig. 3c; the theoretical values of the HOI measures computed in the limit cases $a_{31} = 0$ and $a_{31} = 0.3$ are depicted in Fig. 4a, right.

The process was implemented by feeding the VAR model of Eq. (8) with realizations of five independent Gaussian white noises with unit variance. For each setting obtained varying a_{31} from 0 to 0.3 in steps of 0.03, the simulation was run 100 times changing the length of the generated time series ($N \in \{250, 500, 1000\}$). For each realization, the OIR-gradient, local OIR, and OIR measures were estimated from the VAR parameters identified using least squares

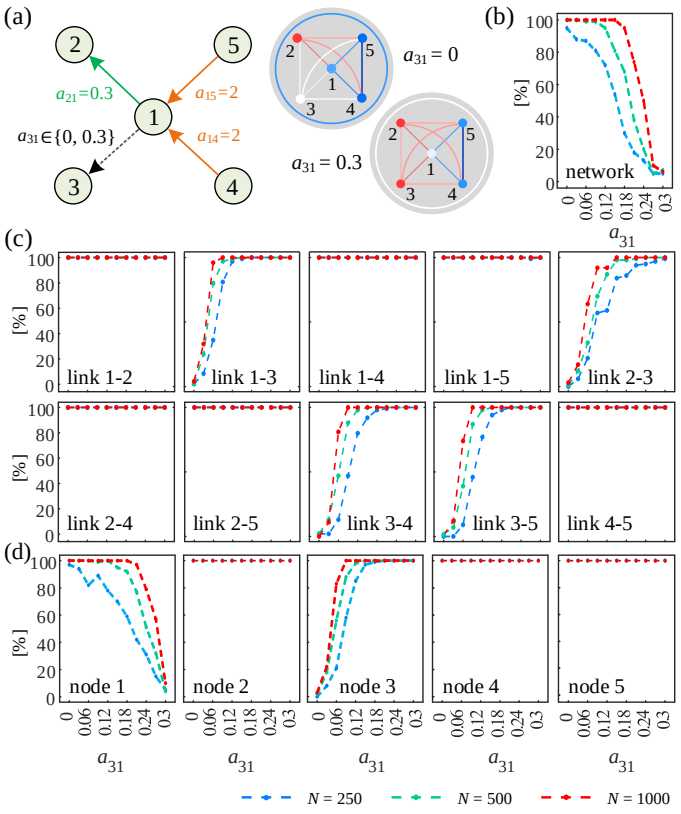

Fig. 4. Practical analysis of HOIs in a simulated network configured as in (a), with the coefficient a_{31} modulated to move from a network with an isolated node exhibiting net synergy to a fully connected network exhibiting synergy/redundancy balance (a, right). When the HOI measures are computed from realizations of the network process varying the time series length N and the coupling coefficient $a31$, the percentage over 100 realizations of statistically significant estimates detected via the bootstrap data analysis are shown in (b) for the OIR of the whole network, in (c) for the local OIR of each link, and in (d) for the OIR-gradient of each node.

estimation as described in Sect. 2.3 (order of the full model: $p = 1$; order of the restricted models: $q = 20$ [27]). Then, the statistical significance of each HOI measure was assessed individually for each simulated time series using the bootstrap method described in Sect. 2.4, implemented over 100 surrogates with significance level $\alpha = 0.05$.

The HOI measures were estimated with minimal bias (OIR-gradient: 0.03 for $N = 250$, 0.02 for $N = 500$, 0.01 for $N = 1000$; local OIR: 0.02 for $N = 250$, 0.01 for $N = 500$, 0.01 for $N = 1000$; OIR: 0.05 for $N = 250$, 0.03 for $N = 500$, 0.02 for $N = 1000$; global average across nodes, links and conditions) and with standard deviation decreasing with the time series length (OIR-gradient: 0.04 for $N = 250$, 0.03 for $N = 500$, 0.02 for $N = 1000$; local OIR: 0.03 for $N = 250$, 0.02 for $N = 500$, 0.01 for $N = 1000$; OIR: 0.07 for $N = 250$, 0.04 for $N = 500$, 0.03 for $N = 1000$; global average across nodes, links and conditions).

The percentage of realizations for which the HOI measures were detected as statistically significant at varying the coupling coefficient a_{31} is reported in Fig. 4b for the OIR computed for the whole network, in Fig. 4c for the local OIR computed across links, and in Fig. 4d for the OIR-gradient computed across nodes. The variation of the coefficient a_{31} leads to a gradual transition of the network

structure from isolation of node 3 to its connection to node 1, which is associated with the rise of node-wise and link-wise HOIs involving node 3, to the dampening of synergistic node-wise HOIs involving node 1, and to the shift from synergistic to balanced network-wise HOIs (see Fig. 4a, right). These transitions were empirically supported by the progressive increase of the percentage of OIR-gradient and local OIR estimates involving node 3 that were identified as statistically significant, rising from the nominal 5 % to 100 % (Fig. 4d,c), as well as by the progressive decrease of the percentage of statistically significant global OIR estimates, decreasing from 100% to 5% (Fig. 4b); these variations were detected more rapidly for longer time series. On the contrary, the node-wise and link-wise HOIs not involving node 3 remained unaffected by these transitions, and their redundant or synergistic nature was detected with 100% sensitivity for all time series lengths.

4 Application to Dynamic Cardiovascular Networks

This section presents the application of the proposed framework to the physiological network related to the short-term neural control of cardiovascular oscillations. The network is analyzed in the resting state and during orthostatic and mental stress, measuring the beat-to-beat variability series representative of heart rate, arterial pressure, cardiac output and peripheral vascular resistance [39]. We first describe LOIs analyzing node activity and pairwise connectivity through the ER and MIR measures, and then move to HOIs assessed at different levels of resolution via the OIR, the local OIR and the OIR-gradient. Our focus is on investigating how different higher-order cardiovascular networks emerge from lower-order dynamics across physiological states.

4.1 Data and Experimental Protocol

We re-analyze a dataset previously collected to study the effects of postural stress and mental stress on cardiovascular regulation in healthy subjects [39]. While the original work included a larger group, here we consider a subset of participants for whom the physiological time series of interest were successfully collected in all experimental conditions. Specifically, five physiological time series were measured on a beat-to-beat basis from the electrocardiogram (ECG), finger arterial blood pressure (ABP), and impedance cardiography (ICG) signals, recorded simultaneously in 26 paticipants and digitized at 1 KHz in the resting supine position (R), during postural stress induced by passive head-up tilt at a 45° angle (T), and during mental stress induced by performing arithmetic tests in the supine position (M). The five analyzed series, constituting realizations of the processes $X = \{X_1, \ldots, X_5\}$ describing the cardiovascular network, were the heart period (HP, process $X_1 = H$), the systolic pressure (SP, process $X_2 = S$), the diastolic pressure (DP, process $X_3 = D$), the cardiac output (CO, process $X_4 = C$), and the peripheral vascular resistance (PR, process $X_5 = P$). These series were derived according to a well-established measurement convention [21], [27], [39]. In detail, the n^{th} sample ($n = 1, \ldots, 300$) of each series was obtained as follows: H_n was taken as the duration of the interval between two consecutive R peaks of the ECG signal; S_n was taken as the maximum value of the ABP signal measured inside H_n; D_n was taken as the minimum value of the ABP signal measured between the occurrence times of S_n and S_{n+1}; $C_n = 60 \cdot (V_n/H_{n-1})$, where V_n is the stroke volume sequence obtained from the ICG signal within H_n; and $P_n = M_n/C_n$, where M_n is the mean ABP measured as the average ABP between the occurrence times of D_{n-1} and D_n. Further details about the protocol and the measurement can be found in [18], [39].

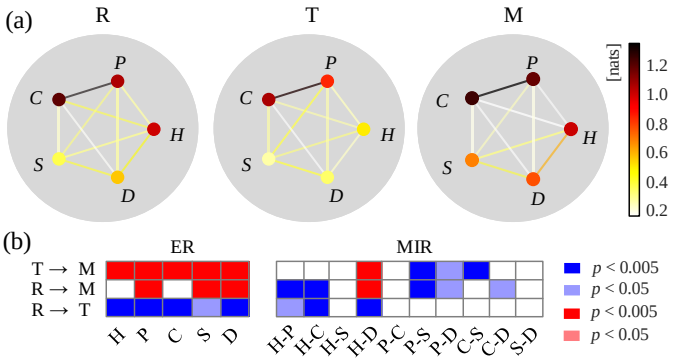

Fig. 5. Lower-order interactions within and between the $N = 5$ processes of heart period H, systolic pressure S, diastolic pressure D, cardiac output C, and peripheral resistance P. (a) Color-coded maps depicting the median values across subjects of the ER (node color) and of the MIR (link color) computed in the resting state (R) and during stress conditions induced by head-up tilt (T) and mental arithmetics (M). (b) Statistically significant differences (blue boxes, decreasing values; red boxes, increasing values) between median values of the ER and MIR distributions (comparisons: R → T, R → M, T → M), assessed by the Wilcoxon signed-rank test.

4.2 Data Analysis and Results

For each subject and condition, each time series was normalized by subtracting the mean and dividing by the standard deviation. The analysis was then performed following the procedure described in Sects. 2.2 and 2.3, optimizing the order p of the full VAR model through the Bayesian criterion [33] and using q = 20 lags to identify restricted VAR models [18]. Statistical validation of MIR and OIR was performed according to Sect. 2.4, generating 100 surrogate and bootstrap time series and setting a significance level $\alpha = 0.05$.

The networks of LOIs obtained computing the ER of each cardiovascular process (H, D, S, C, P) and the MIR between each pair of processes in each physiological condition (R, T, M) are depicted in Fig. 5a as color-coded values of nodes and links (median over 26 subjects), while the statistically significant differences between pairs of conditions are reported in Fig. 5b. The analysis of the individual node dynamics performed by the ER measure documented a statistically significant decrease from R to T and a significant increase from T to M for each process, as well as significant increase for PR, SP and DP from R to M. These findings indicate reduced complexity (higher regularity) of all physiological variability series during postural stress compared to rest, which can be ascribed to the expected parasympathetic control inhibition reflected mostly in heart period dynamics and the sympathetic nervous activity activation related to postural stress producing a rise of low-frequency regular os-

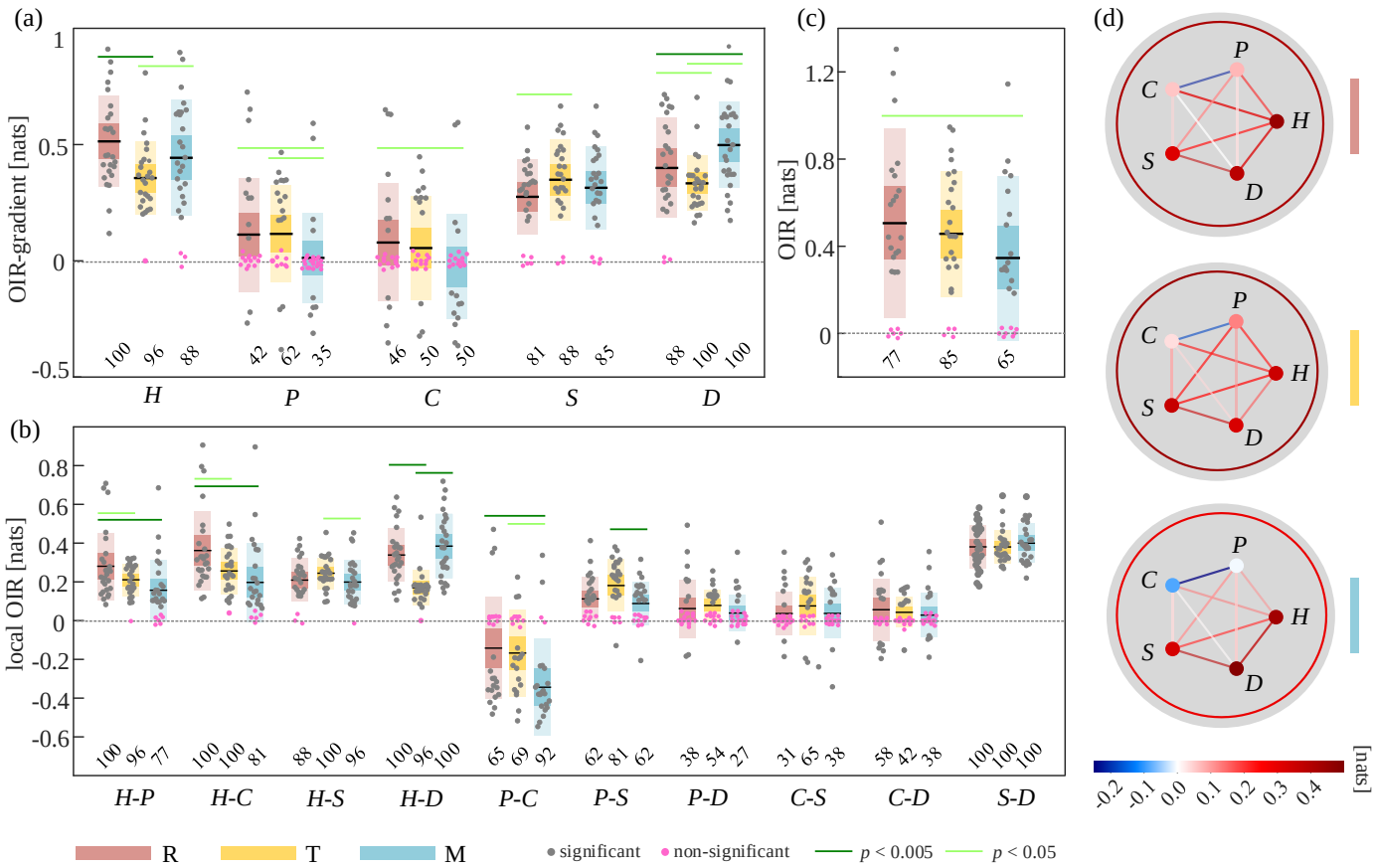

Fig. 6. Higher-order interactions in the cardiovascular network mapped by the $N = 5$ processes of heart period H, systolic pressure S, diastolic pressure D, cardiac output C, and peripheral resistance P, quantified at the level of nodes by the OIR-gradient (a), of links by the local OIR (b), and of the whole network by the OIR (c), and expressed distributions across subjects (boxplot and individual values) obtained during resting (R), head-up tilt (T) and mental arithmetic (M) conditions. The numbers below the distributions indicate the percentage of subjects for whom the estimates of HOIs measures were evaluated as statistically significant through the bootstrap data analysis (gray dots: significant values, purple dots: non-significant); green lines denote statistically significant differences between pairs of distributions (comparisons: R vs. T, R vs. M, T vs. M) assessed with the Wilcoxon signed-rank test. (d) Color-coded maps depicting the median values across subjects of the OIR-gradient (node color), local OIR (link color), and OIR (color of the external circle) computed in the R, T, and M conditions.

cillations [40], [41]. On the other hand, mental stress induced higher complexity of arterial pressure and vascular resistance series also if compared to the resting state, suggesting higher involvement of sympathetic vascular control and a decreased baroreflex buffering of blood pressure oscillations mostly reflecting reflex parasympathetic control inhibition. As regards the MIR, it was always detected as statistically significant using the iAAFT surrogate procedure, revealing a fully connected network of pairwise physiological interactions. The strongest coupling in the network was detected between PR and CO for each condition, resulting from the tight inverse relation between these two processes [39]. The MIR was high also for the links SP-HP, HP-DP and SP-DP, reflecting typical mechanisms of cardiovascular coupling like the baroreflex feedback (SP $\rightarrow$ HP) and the mechanical feed-forward (HP $\rightarrow$ SP), the cardiac run-off (HP $\rightarrow$ DP), and the close association between DP and neighboring SP values (DP $\rightarrow$ SP and SP $\rightarrow$ DP) [20], [21], [42]. The undirected coupling strength reflected by the MIR for these links was rather stable across conditions, except for the link HP-DP whose strength decreased during T and increased during M; this suggests that postural stress and mental stress have different impact on the dynamics resulting from the cardiac run-off mechanism [21]. The remaining links, i.e. those involving the variability of PR or CO together with the other processes, were less strong, though still statistically significant; for these links, the MIR decreased with mental stress and the ER increased, documenting a case of higher complexity associated with less coupled dynamics [43].

Fig. 6 depicts the results of the analysis of HOIs, reporting the distributions of OIR-gradient (a), local OIR (b) and OIR (c), computed for each node, link and for the whole network in the three conditions, as well as the HOI networks depicted using color-coded maps of the median values of each measure computed across subjects (d). The network-wise analysis of HOIs suggests the presence of dominant redundancy in the analyzed cardiovascular network, documented by the positive values of the OIR measure in all conditions (Fig. 6c). The analysis performed with different resolution reveals an heterogeneous distribution of HOIs at the levels of nodes and links. Fig. 6 a, b show that: (i) the OIR-gradient of HP and the local OIR of the related links (i.e., HP-PR, HP-CO, HP-SP, HP-DP), as well as the OIR-gradients of DP and SP and their related local OIR (SP-DP), are consistently redundant and significant for the majority of subjects; (ii) the OIR-gradient of PR and CO and

the local OIR of the links PR-SP, PR-DP, CO-SP, CO-DP are more balanced and significant in about half of the subjects; (iii) the local OIR involving PR and CO displays evident synergy, statistically significant in most subjects. The overall redundancy observed in the analyzed network is likely arising from the action of common physiological drivers such as respiration or sympathetic activity that modulate several processes simultaneously [18], [19], [44], [45]. On the other hand, the observed heterogeneity in the distribution of HOIs across the nodes of the physiological network is an indicator of the coexistence of common drive mechanisms like those related to respiration affecting both heart rate and arterial pressure variability [45], [46], and of common target mechanisms like those associated to the influence of the dynamics of vascular resistance and stroke volume on arterial pressure [18], [47]. Notably, these different mechanisms associated respectively to local redundancy and local synergy are detected in the presence of comparably strong MIR values, thus pinpointing how HOI measures can detect behaviors that remain hidden to LOI descriptors.

The transition from rest to stress determined a reconfiguration of the networks of HOIs, which exhibit a general tendency towards lower net redundancy or the emergence of net synergy. In particular, postural stress is associated with a marked reduction of the OIR-gradient relevant to HP and DP, as well as of the corresponding local OIR (HP-DP). Similarly, mental stress results in a significant reduction of the OIR-gradient relevant to PR and CO, as well as of their local OIR (PR-CO). Moreover, the local OIR of the links HP-PR and HP-CO decreased significantly with both types of stressor. At the network-wise level, the values of net redundancy were comparable at rest and during postural stress, and significantly lower during mental stress (Fig. 6c, d). Methodologically, a decrease of redundancy and/or an increase in synergy occur when HOI measures like the OIR-gradient or the local OIR are computed for nodes acting as sources of information that is injected in the network when their dynamics are considered (see simulations, Fig. 1e, f). Our results show that this happens for HP and DP during head-up tilt, and for PR and CO during the execution of mental calculations. This suggests that synergistic mechanical effects like the cardiovascular feedforward (HP $\rightarrow$ SAP) [48] are strengthened by postural stress, and synergistic autonomic effects like the sympathetic-driven modulation of the contractility of heart and vessels influencing arterial pressure (effects CO $\rightarrow$ SAP and PR $\rightarrow$ SAP) [49] are strengthened by mental stress. These modulations induced by stress on the OIR gradient and local OIR measures, together with the variations observed for the ER and MIR measures, support the view that a combined analysis of LOI and HOI in cardiovascular networks is needed to provide a clearer picture of the underlying physiology.

5 Conclusions and Perspectives

This work introduces a framework for evaluating higher-order statistical dependencies in dynamic network systems, explicitly designed to explore different levels of resolution. The framework incorporates dynamic implementations of the O-information, its local counterpart, and its gradient, which are intended to quantify HOIs respectively for the network as a whole, for each link, and for each node. As such, it allows not only to identify the emergent redundant or synergistic character of a dynamic network system, but also to assess how the synergy/redundancy balance is distributed across links and nodes. The existing approaches proposed to assess spatially-resolved high-order behaviors, which focus on computing HOI measures on subsets of nodes (multiplets) of the network at hand [15], [24], analyze each given multiplet ignoring the rest of the network, and are impractical to implement as the number of multiplets to analyze grows exponentially with the network size. These drawbacks are overcame by our framework, as it considers the dynamics of all nodes at any level of resolution and it provides a HOI measure for each level: the OIR of all processes as collective network-wise measure, the local OIR between two processes and the rest of the network as link-wise measure, and the OIR-gradient between one process and the rest of the network as node-wise measure. Ultimately, merging these different types of information through the standard formalism of network depiction allows to efficiently represent high-order interactions as networks. This compact, yet comprehensive approach keeps the complexity of the network representation low, thus favoring implementation and accessibility of the proposed framework.

The potentiality of the new framework was first demonstrated in theoretical examples of dynamic networks modeled as VAR processes, for which exact calculations of the HOIs measures were provided under different network configurations. The analysis of simulated network systems demonstrated the importance of using the dynamic framework to fully capture HOIs when the analyzed processes have non-trivial temporal statistical structure, while in this case the standard static analysis computing HOIs for random variables [14] may fail to detect higher-order effects. Further, simulations emphasized that higher-order measures not only provide additional information about the emergent synergistic or redundant behaviors of network systems compared to standard lower-order descriptors, but also enable a clear distinction among the different underlying connectivity patterns. Indeed, we have shown how higher-order behaviors of a network system, even as simple as a first-order linear process, do not necessarily rely on higher-order mechanisms [8]. In fact, simple pairwise linear couplings between random processes can give rise either to fully redundant HOIs related to common driver effects, to fully synergistic HOIs related to common target effects, or to mixed redundant and synergistic HOIs related to coexisting common driver, cascade and common target effects [50]. The latter situation, which is very common in complex networks with intricate (though low-order) connections such as those found in computational physiology [5], [18], [21], underlines the importance to explore higher-order behaviors at different levels of resolution. In particular, we have shown that the coexistence of redundant and synergistic HOIs can be often elicited only by going beyond the global assessment provided by the OIR through the use of its link-wise or node-wise versions (see, e.g., Fig. 3g, h). The implementation of the HOIs measures in short-length realizations of the processes, complemented by the statistical validation based on surrogate/bootstrap time series, have documented the

feasibility of their estimation in practical contexts.

The proposed framework was then tested in a physiological application, extending previous analyses that were limited to studying three-variate interactions [44], [45], [46] and more recent implementations focused on network reconstruction [18]. Our analysis showed how HOI networks can offer additional and sometimes complementary information compared to standard networks which exclusively depict LOIs focusing on individual node activity and pairwise functional connectivity. In the observed cardiovascular networks, we documented the existence of heterogeneous HOIs among dynamic physiological processes monitored at rest and during stress, identifying respectively the heart period and the diastolic pressure, and the cardiac output and the peripheral resistance, as the processes evoking lower net redundancy during postural stress and higher net synergy during mental stress, also identifying the putative neuromechanical mechanisms associated with network reconfiguration [10], [18], [20], [48], [49]. These results have physiological relevance related to how physiological mechanisms can be interpreted in terms of the high-order behaviors that they produce in cardiovascular oscillations, but can also have clinical importance related to the extraction of HOI-based biomarkers reflecting system-wise pathological alterations [51], as well as practical relevance thanks to the fact that multivariate physiological time series are nowadays easy to record in daily life settings and can be exploited to assess the cardiovascular control in several contexts including stress monitoring [52], aging [53], or exercise [54].

Importantly, thanks to its information-theoretic foundation and to the data-driven implementation, our framework is very general and can be applied virtually to any multivariate dataset featuring time series with temporal auto- and cross-correlations. In fact, the applicability of our approach for depicting HOI networks is broad and extends far beyond the description of cardiovascular networks, encompassing dynamic networks in fields where the node activity can be represented by random processes, such as neuroscience, electronics, climatology, social sciences, finance, and others [10], [19], [55], [56], [57]. Moreover, the framework is highly flexible and lends itself to extensions that will further broaden its applicability, including its recent and ongoing model-free [58], time-varying [31] and spectral [17] formulations, that will allow to capture complex high-order behaviors and dissect non-stationary and frequency-specific HOIs that are relevant to a big variety of biological and engineered networks.

APPENDIX

The computation of HOI measures for a network of random variables relies on the classic information-theoretic concept of entropy [22] and on the more recent concept of O-information (OI) [14]. In particular, the OI of a vector random variable $V = \{V_1, \dots, V_N\}$ is defined as [14]:

$$\Omega(V) = (N-2)H(V) + \sum_{j=1}^{N}[H(V_j) - H(V^j)], \qquad (20)$$

where $V^j = V \backslash V_j$ and $H(\cdot)$ denotes entropy. Moreover, the OI-gradient obtained including the variable V_j into the set of remaining variables V^j can be defined as [15]:

$$\Delta(V_j; V^j) = \Omega(V) - \Omega(V^j), \qquad (21)$$

while the local OI between the variables V_i and V_j, and the remaining variables V^{ij} [14] is an interaction information [13] which can be expressed as:

$$\begin{aligned} I(V_i; V_j; V^{ij}) = H(V) + H(V_i) + H(V_j) + H(V^{ij}) \\ - H(V^i) - H(V^j) - H(V_{ij}), \end{aligned} \qquad (22)$$

with $V_{ij} = \{V_i, V_j\}$. Remarkably, all measures in (20-22) can be expressed as linear combinations of entropies for variables of different dimension taken from V. In the present work, these OI-based measures are computed to assess static HOIs in the network of random processes $X = \{X_1, \dots, X_N\}$ simply by applying Eqs. (20-22) to the vector variable sampling the processes at the same time n, i.e. taking $V = X_n$. The practical computation of these static measures from VAR processes is based on the assumption of joint Gaussianity of V, according to which the entropy of the generic d-dimensional variable $W \subseteq V$ is given by:

$$H(W) = \frac{1}{2}\log(2\pi e)^d |\mathbf{\Sigma}_W|, \qquad (23)$$

where W can be any of the variables appearing in (20-22) and the covariance $\mathbf{\Sigma}_W$ is a sub-matrix of the covariance matrix of the process, $\mathbf{\Sigma}_V = \mathbf{\Sigma}_X = \mathbb{E}[X_n X_n^\intercal]$; the latter can be derived from the VAR parameters solving the Yule-Walker equation (15) for $k = 0$.

SOFTWARE AVAILABILITY

The Matlab functions that perform the HOIs framework are available for free download at:
https://github.com/mijatovicg/HOIs-as-networks.

REFERENCES

[1] S. Boccaletti, V. Latora, Y. Moreno, M. Chavez, and D.-U. Hwang, "Complex networks: Structure and dynamics," *Physics reports*, vol. 424, no. 4-5, pp. 175–308, 2006.

[2] A. R. Benson, D. F. Gleich, and J. Leskovec, "Higher-order organization of complex networks," *Science*, vol. 353, no. 6295, pp. 163–166, 2016.

[3] L. Minati, L. Faes, M. Frasca, P. Oswiecimka, and S. Drod, "Apparent remote synchronization of amplitudes: A demodulation and interference effect," *Chaos: An Interdisciplinary Journal of Nonlinear Science*, vol. 28, no. 6, 2018.

[4] G. Woodward, J. P. Benstead, O. S. Beveridge, J. Blanchard, T. Brey, L. E. Brown, W. F. Cross, N. Friberg, T. C. Ings, U. Jacob *et al.*, "Ecological networks in a changing climate," in *Advances in ecological research*. Elsevier, 2010, vol. 42, pp. 71–138.

[5] A. Bashan, R. P. Bartsch, J. W. Kantelhardt, S. Havlin, and P. C. Ivanov, "Network physiology reveals relations between network topology and physiological function," *Nature communications*, vol. 3, no. 1, p. 702, 2012.

[6] D. S. Bassett and O. Sporns, "Network neuroscience," *Nature neuroscience*, vol. 20, no. 3, pp. 353–364, 2017.

[7] F. Battiston, G. Cencetti, I. Iacopini, V. Latora, M. Lucas, A. Patania, J.-G. Young, and G. Petri, "Networks beyond pairwise interactions: Structure and dynamics," *Physics Reports*, vol. 874, pp. 1–92, 2020.

[8] F. E. Rosas, P. A. Mediano, A. I. Luppi, T. F. Varley, J. T. Lizier, S. Stramaglia, H. J. Jensen, and D. Marinazzo, "Disentangling high-order mechanisms and high-order behaviours in complex systems," *Nature Physics*, vol. 18, no. 5, pp. 476–477, 2022.

[9] I. Iacopini, G. Petri, A. Barrat, and V. Latora, "Simplicial models of social contagion," *Nature communications*, vol. 10, no. 1, p. 2485, 2019.

[10] L. V. Gambuzza, F. Di Patti, L. Gallo, S. Lepri, M. Romance, R. Criado, M. Frasca, V. Latora, and S. Boccaletti, "Stability of synchronization in simplicial complexes," *Nature communications*, vol. 12, no. 1, p. 1255, 2021.

[11] P. L. Williams and R. D. Beer, "Nonnegative decomposition of multivariate information," *arXiv preprint arXiv:1004.2515*, 2010.

[12] J. T. Lizier, N. Bertschinger, J. Jost, and M. Wibral, "Information decomposition of target effects from multi-source interactions: Perspectives on previous, current and future work," p. 307, 2018.

[13] W. McGill, "Multivariate information transmission," *Transactions of the IRE Professional Group on Information Theory*, vol. 4, no. 4, pp. 93–111, 1954.

[14] F. E. Rosas, P. A. Mediano, M. Gastpar, and H. J. Jensen, "Quantifying high-order interdependencies via multivariate extensions of the mutual information," *Physical Review E*, vol. 100, no. 3, p. 032305, 2019.

[15] S. Stramaglia, T. Scagliarini, B. C. Daniels, and D. Marinazzo, "Quantifying dynamical high-order interdependencies from the o-information: an application to neural spiking dynamics," *Frontiers in Physiology*, vol. 11, p. 595736, 2021.

[16] L. Faes, G. Mijatovic, Y. Antonacci, R. Pernice, C. Barà, L. Sparacino, M. Sammartino, A. Porta, D. Marinazzo, and S. Stramaglia, "A new framework for the time-and frequency-domain assessment of high-order interactions in networks of random processes," *IEEE Transactions on Signal Processing*, vol. 70, pp. 5766–5777, 2022.

[17] L. Sparacino, Y. Antonacci, G. Mijatovic, and L. Faes, "Measuring hierarchically-organized interactions in dynamic networks through spectral entropy rates: theory, estimation, and illustrative application to physiological networks," *arXiv preprint arXiv:2401.11327*, 2024.

[18] G. Mijatovic, L. Sparacino, Y. Antonacci, M. Javorka, D. Marinazzo, S. Stramaglia, and L. Faes, "Assessing high-order links in cardiovascular and respiratory networks via static and dynamic information measures," *IEEE Open Journal of Engineering in Medicine and Biology*, 2024.

[19] T. Scagliarini, L. Sparacino, L. Faes, D. Marinazzo, and S. Stramaglia, "Gradients of o-information highlight synergy and redundancy in physiological applications," *Frontiers in Network Physiology*, vol. 3, p. 1335808, 2024.

[20] M. A. Cohen and J. A. Taylor, "Short-term cardiovascular oscillations in man: measuring and modelling the physiologies," *The Journal of physiology*, vol. 542, no. 3, pp. 669–683, 2002.

[21] M. Javorka, J. Krohova, B. Czippelova, Z. Turianikova, Z. Lazarova, K. Javorka, and L. Faes, "Basic cardiovascular variability signals: mutual directed interactions explored in the information domain," *Physiological Measurement*, vol. 38, no. 5, p. 877, 2017.

[22] T. M. Cover, *Elements of information theory*. John Wiley & Sons, 1999.

[23] T. E. Duncan, "On the calculation of mutual information," *SIAM Journal on Applied Mathematics*, vol. 19, no. 1, pp. 215–220, 1970.

[24] D. Marinazzo, J. Van Roozendaal, F. E. Rosas, M. Stella, R. Comolatti, N. Colenbier, S. Stramaglia, and Y. Rosseel, "An information-theoretic approach to build hypergraphs in psychometrics," *Behavior Research Methods*, vol. 56, no. 7, pp. 8057–8079, 2024.

[25] H. Lütkepohl, *New introduction to multiple time series analysis*. Springer Science & Business Media, 2005.

[26] H. Wold, "A study in the analysis of stationary time series," Ph.D. dissertation, Almqvist & Wiksell, 1938.

[27] L. Faes, A. Porta, G. Nollo, and M. Javorka, "Information decomposition in multivariate systems: definitions, implementation and application to cardiovascular networks," *Entropy*, vol. 19, no. 1, p. 5, 2017.

[28] L. Barnett and A. K. Seth, "Granger causality for state-space models," *Physical Review E*, vol. 91, no. 4, p. 040101, 2015.

[29] ——, "The mvgc multivariate granger causality toolbox: a new approach to granger-causal inference," *Journal of neuroscience methods*, vol. 223, pp. 50–68, 2014.

[30] Y. Antonacci, L. Astolfi, G. Nollo, and L. Faes, "Information transfer in linear multivariate processes assessed through penalized regression techniques: validation and application to physiological networks," *Entropy*, vol. 22, no. 7, p. 732, 2020.

[31] Y. Antonacci, C. Barà, A. Zaccaro, F. Ferri, R. Pernice, and L. Faes, "Time-varying information measures: an adaptive estimation of information storage with application to brain-heart interactions," *Frontiers in Network Physiology*, vol. 3, p. 1242505, 2023.

[32] H. Akaike, "A new look at the statistical model identification," *IEEE transactions on automatic control*, vol. 19, no. 6, pp. 716–723, 1974.

[33] G. Schwarz, "Estimating the dimension of a model," *The annals of statistics*, pp. 461–464, 1978.

[34] B. Efron, "Bootstrap methods: another look at the jackknife," *The Annals of Statistics*, vol. 7, pp. 1–26, 1979.

[35] L. Sparacino, L. Faes, G. Mijatović, G. Parla, V. Lo Re, R. Miraglia, J. de Ville de Goyet, and G. Sparacia, "Statistical approaches to identify pairwise and high-order brain functional connectivity signatures on a single-subject basis," *Life*, vol. 13, no. 10, p. 2075, 2023.

[36] T. Schreiber and A. Schmitz, "Improved surrogate data for nonlinearity tests," *Physical review letters*, vol. 77, no. 4, p. 635, 1996.

[37] F. E. Rosas, P. A. Mediano, M. Gastpar, and H. J. Jensen, "Quantifying high-order interdependencies via multivariate extensions of the mutual information," *Physical Review E*, vol. 100, no. 3, p. 032305, 2019.

[38] M. Ontivero-Ortega, L. Faes, J. M. Cortes, D. Marinazzo, and S. Stramaglia, "Assessing high-order effects in feature importance via predictability decomposition," *arXiv preprint arXiv:2412.09964*, 2024.

[39] J. Krohova, L. Faes, B. Czippelova, R. Pernice, Z. Turianikova, R. Wiszt, N. Mazgutova, A. Busacca, and M. Javorka, "Vascular resistance arm of the baroreflex: methodology and comparison with the cardiac chronotropic arm," *Journal of Applied Physiology*, vol. 128, no. 5, pp. 1310–1320, 2020.

[40] L. Faes, M. Gómez-Extremera, R. Pernice, P. Carpena, G. Nollo, A. Porta, and P. Bernaola-Galván, "Comparison of methods for the assessment of nonlinearity in short-term heart rate variability under different physiopathological states," *Chaos: An Interdisciplinary Journal of Nonlinear Science*, vol. 29, no. 12, p. 123114, 2019.

[41] G. Mijatovic, R. Pernice, A. Perinelli, Y. Antonacci, A. Busacca, M. Javorka, L. Ricci, and L. Faes, "Measuring the rate of information exchange in point-process data with application to cardiovascular variability," *Front. Netw. Physiol. 1: 765332. doi: 10.3389/fnetp*, 2022.

[42] L. Faes, G. Nollo, and A. Porta, "Mechanisms of causal interaction between short-term rr interval and systolic arterial pressure oscillations during orthostatic challenge," *Journal of applied physiology*, vol. 114, no. 12, pp. 1657–1667, 2013.

[43] A. Porta, L. Faes, V. Bari, A. Marchi, T. Bassani, G. Nollo, N. M. Perseguini, J. Milan, V. Minatel, A. Borghi-Silva *et al.*, "Effect of age on complexity and causality of the cardiovascular control: comparison between model-based and model-free approaches," *PloS one*, vol. 9, no. 2, p. e89463, 2014.

[44] A. Porta, V. Bari, B. De Maria, A. C. Takahashi, S. Guzzetti, R. Colombo, A. M. Catai, F. Raimondi, and L. Faes, "Quantifying net synergy/redundancy of spontaneous variability regulation via predictability and transfer entropy decomposition frameworks," *IEEE Transactions on Biomedical Engineering*, vol. 64, no. 11, pp. 2628–2638, 2017.

[45] A. Porta, R. Maestri, V. Bari, B. De Maria, B. Cairo, E. Vaini, M. T. La Rovere, and G. D. Pinna, "Paced breathing increases the redundancy of cardiorespiratory control in healthy individuals and chronic heart failure patients," *Entropy*, vol. 20, no. 12, p. 949, 2018.

[46] A. Porta, F. Gelpi, V. Bari, B. Cairo, B. De Maria, D. Tonon, G. Rossato, M. Ranucci, and L. Faes, "Categorizing the role of respiration in cardiovascular and cerebrovascular variability interactions," *IEEE Transactions on Biomedical Engineering*, vol. 69, no. 6, pp. 2065–2076, 2021.

[47] M. Nardone, A. V. Incognito, and P. J. Millar, "Evidence for pressure-independent sympathetic modulation of central pulse wave velocity," *Journal of the American Heart Association*, vol. 7, no. 3, p. e007971, 2018.

[48] M. Javorka, B. Czippelova, Z. Turianikova, Z. Lazarova, I. Tonhajzerova, and L. Faes, "Causal analysis of short-term cardiovascular variability: state-dependent contribution of feedback and feedforward mechanisms," *Medical & biological engineering & computing*, vol. 55, pp. 179–190, 2017.

[49] G. D. Thomas, "Neural control of the circulation," *Advances in physiology education*, vol. 35, no. 1, pp. 28–32, 2011.

[50] D. P. MacKinnon and S. J. Lamp, "A unification of mediator,

confounder, and collider effects," *Prevention Science*, vol. 22, no. 8, pp. 1185–1193, 2021.
[51] P. C. Ivanov, K. K. Liu, and R. P. Bartsch, "Focus on the emerging new fields of network physiology and network medicine," *New journal of physics*, vol. 18, no. 10, p. 100201, 2016.
[52] M. Zanetti, T. Mizumoto, L. Faes, A. Fornaser, M. De Cecco, L. Maule, M. Valente, and G. Nollo, "Multilevel assessment of mental stress via network physiology paradigm using consumer wearable devices," *Journal of Ambient Intelligence and Humanized Computing*, vol. 12, pp. 4409–4418, 2021.
[53] R. Romero-Ortuño, N. Martínez-Velilla, R. Sutton, A. Ungar, A. Fedorowski, R. Galvin, O. Theou, A. Davies, R. B. Reilly, J. Claassen *et al.*, "Network physiology in aging and frailty: the grand challenge of physiological reserve in older adults," *Frontiers in Network Physiology*, vol. 1, p. 712430, 2021.
[54] F. Iellamo, "Neural mechanisms of cardiovascular regulation during exercise," *Autonomic Neuroscience*, vol. 90, no. 1-2, pp. 66–75, 2001.
[55] U. Alvarez-Rodriguez, F. Battiston, G. F. de Arruda, Y. Moreno, M. Perc, and V. Latora, "Evolutionary dynamics of higher-order interactions in social networks," *Nature Human Behaviour*, vol. 5, no. 5, pp. 586–595, 2021.
[56] Y. Antonacci, L. Minati, D. Nuzzi, G. Mijatovic, R. Pernice, D. Marinazzo, S. Stramaglia, and L. Faes, "Measuring high-order interactions in rhythmic processes through multivariate spectral information decomposition," *IEEE Access*, vol. 9, pp. 149 486–149 505, 2021.
[57] A. I. Luppi, F. E. Rosas, P. A. Mediano, D. K. Menon, and E. A. Stamatakis, "Information decomposition and the informational architecture of the brain," *Trends in Cognitive Sciences*, 2024.
[58] D. A. Ehrlich, K. Schick-Poland, A. Makkeh, F. Lanfermann, P. Wollstadt, and M. Wibral, "Partial information decomposition for continuous variables based on shared exclusions: Analytical formulation and estimation," *Physical Review E*, vol. 110, no. 1, p. 014115, 2024.

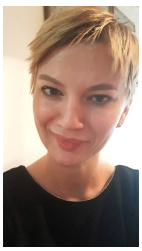

Gorana Mijatovic (Member, IEEE) received B.Sc. degree and M.Sc. degree in Electrical engineering in 2009, 2010, and the Ph.D. degree in Electrical Engineering in 2018, form the University of Novi Sad, Serbia. Her current position is Associate Professor at Department for power, electronics and telecommunications of Faculty of Technical Sciences, University of Novi Sad, Serbia. Her research activity includes computational neuroscience, network physiology, complex systems and network dynamics; within these fields, she has authored more than 60 papers in peer-reviewed international journals and conference proceedings.

Yuri Antonacci (Member, IEEE) was born in Rome, Italy, in 1989. He received his M.Sc. degree (cum laude) in Biomedical Engineering and his Ph.D. in Bioengineering from the University of Rome "La Sapienza", Italy, in 2016 and 2021, respectively. From 2021 to 2023, he was a Postdoctoral Research Fellow with the Department of Physics and Chemistry "Emilio Segrè" and the Department of Engineering at the University of Palermo, where he is currently an Assistant Professor. His main research interests include time series analysis, digital signal processing, and system modeling applied to physiological data.

Michal Javorka (M.D., Ph.D., 2002, full professor since 2016) is a physiologist at the Dept. of Physiology, Comenius University, Jessenius Faculty of Medicine in Martin, Slovakia). Research interests: cardiovascular autonomic control, cardiorespiratory interactions, hemodynamics, network physiology, biomedical signal analysis, complexity analysis, nonlinear dynamics. Publications: $>$ 150 papers in peer-reviewed international journals and conference proceedings, $>$ 2400 citations, h-index 30 (Scopus).

Daniele Marinazzo is a statistical physicist working mainly in the neurosciences. The research activity of his group focuses on methodological and computational aspects of neuroscience research, and on the dynamical networks subserving function. His group develops new techniques for inferring connectivity architectures from the dynamics of the recorded data, in challenging cases of short, noisy and redundant time series, as those encountered in neuroimaging, implementing and validating novel methodologies and applying them, together with already established ones, in several multidisciplinary projects. He is Deputy Editor at PLOS Computational Biology, Co-Editor-in-Chief at Neurons, Behavior, Data analysis, and Theory, and academic editor at Network Neuroscience, NeuroImage, Brain Topography.

Sebastiano Stramaglia is Full Professor in Applied Physics and the head of the Center of Innovative Technologies for Signal Detection and Processing at the University of Bari (Italy). His interests span from Statistical Mechanics to Information Theory for Complex Systems. He contributed to the development to several methodological approaches to analyze network data and complex signals, mainly for biomedical applications. His current research focuses on the analysis of information flow patterns, both at the lowest level (Granger causality, transfer entropy) and at higher order levels of statistical dependencies.

Luca Faes (Senior Member, IEEE) is Professor of Biomedical Engineering at the University of Palermo, Italy, since 2018. He obtained his PhD in Electronic Engineering at the University of Trento (2003). He was with the Dept. of Physics (2004-2013) and the BIOtech Center (2008-2013) of the University of Trento, and with the Bruno Kessler Foundation (FBK, Trento, 2013-2017). He has been visiting scientist at the State University of New York (2007), Worcester Polytechnic Institute (2010), University of Gent (Belgium, 2013), University of Minas Gerais (Brazil, 2015), and Boston University (2016). He is a member of the IEEE Engineering in Medicine and Biology Society (IEEE-EMBS), and of the European Study Group on Cardiovascular Oscillations (ESGCO). He serves as Associate Editor for IEEE Transactions on Biomedical Engineering. His research activity is focused on the development of methods for multivariate time series analysis and system modeling, with applications to cardiovascular neuroscience, brain connectivity and network physiology. Within these fields, he has authored more than 150 peer-reviewed publications, receiving more than 8000 citations (h-index: 51; font: Scholar).